Integrated use of ligand and structure based virtual screening, molecular dynamics, free energy calculation and ADME prediction for the identification of potential PTP1B inhibitors

Bharti Devi
Indian Institute of Technology (B.H.U.)
Sumukh Satyanarayana Vasishta
Indian Institute of Technology (B.H.U.)
Bhanuranjan Das
Indian Institute of Technology (B.H.U.)
Anurag TK Baidya
Indian Institute of Technology (B.H.U.)
Rahul Salmon Rampa
Indian Institute of Technology (B.H.U.)
Manoj Kumar Mahapatra
Kanak Manjari Institute of Pharmaceutical Sciences
Rajnish Kumar (rajnish.phe@iitbhu.ac.in)
Indian Institute of Technology (B.H.U.)

Research Article

Keywords: PTP1B inhibitors, pharmacophore modelling, virtual screening, MD simulation, MM_PBSA

Posted Date: October 18th, 2022

DOI: https://doi.org/10.21203/rs.3.rs-2162440/v1

Additional Declarations: No competing interests reported.

Version of Record: A version of this preprint was published at Molecular Diversity on February 6th, 2023. See the published version at https://doi.org/10.1007/s11030-023-10608-8.

Abstract

Protein tyrosine phosphatases (PTPs) are the group of enzymes that control both cellular activity and the dephosphorylation of tyrosine (Tyr)-phosphorylated proteins. Dysregulation of PTP1B has contributed to numerous diseases including Diabetes Mellitus, Alzheimer's disease, and obesity rendering PTP1B as a legitimate target for therapeutic applications. However, it is highly challenging to target this enzyme because of its highly conserved and positively charged active-site pocket motivating researchers to find novel lead compounds against it. The present work makes use of an integrated approach combining ligand based and structure-based virtual screening to find hit compounds targeting PTP1B. Initially, pharmacophore modelling was performed to find common features like two hydrogen bond acceptors, an aromatic ring and one hydrogen bond donor from the ligands with reported inhibition activity against PTP1B. The dataset of compounds matching with the common pharmacophoric features was filtered to remove Pan-Assay Interference substructure and to match the Lipinski criteria. Then, compounds were further prioritized using molecular docking and top fifty compounds with good binding affinity were selected for ADME predictions. The top five compounds with high solubility, absorption and permeability holding score of -10 to -9.3 kcal/mol along with Ertiprotafib were submitted to all-atom molecular dynamic (MD) studies. The MD studies and binding free energy calculations showed that compound M4, M5 and M8 were having better binding affinity for PTP1B enzyme with ΔG_{total} score of -24.25, -31.47 and -33.81 kcal/mol respectively than other compounds indicating that compound M8 could be a suitable lead compound for PTP1B enzyme inhibition.

1. Introduction

Protein-tyrosine phosphatase 1B (PTP1B) is the first member of the group of protein tyrosine phosphatase enzymes [1]. Protein tyrosine phosphatases (PTPs) are a family of enzymes that control both cellular activity and the dephosphorylation of tyrosine (Tyr)-phosphorylated proteins [2, 3]. Among the 107 PTPs of human genome PTP1B belongs to class I cysteine-based PTP group [4, 5]. Dysregulation of PTP1B has contributed to numerous diseases including Diabetes Mellitus (DM), Alzheimer's disease (AD), obesity etc. [6]. Thus, PTP1B is a promising target for therapeutic applications. However, it is challenging to target this enzyme because of greatly conserved and positively charged active-site pocket motivating researchers to find new lead compounds against this target. DM has become a menace to the world affecting close to 422 million people according to World Health Organization (WHO) [7].

PTP1B plays a vital role in the negative regulation of insulin signaling pathway and inhibiting overexpression of the enzyme may reduce the insulin resistance [8–10]. Evidences suggests that PTP1B knockout mice had improved insulin sensitivity and glucose tolerance, which reassures the above statement [11]. AD is another threat, which affects almost twenty-four million people globally and it primarily affects elders over the age of sixty-five. PTP1B plays a vital role in inhibition of signaling processes like insulin, leptin, mGluR5 and trkB and these pathways are reported to be disturbed in AD [12]. Increased PTP1B activity also prevents the phosphorylation and constitutive inhibition of glycogen synthase kinase 3 Beta (GSK3 Beta) via its inhibition of kinase Akt/PKB. Activity of GSK3 Beta leads to formation of cerebral deposits which are associated with AD and leads to reduced cognitive performance making PTP1B a promising target for the management of AD.

Faulty hypothalamic leptin signaling impairs sensing and processing of satiety signals in obesity, resulting in higher calorie intake and lower energy expenditure. PTP1B dephosphorylates LepR and JAK2 [13, 14]; which are vital components of Leptin signaling pathway, acting as an antagonistic leptin signaling regulator. High-fat diet (HFD) and deletion of the leptin gene make the PTP1B-null mice resistant towards weight gain, indicating that PTP1B inhibition may be an effective way to restore leptin signaling in obese individuals [15].

PTP1B is also considered as an emerging target for the treatment of cancer. Depending on the type of tumor, PTP1B plays a variety of roles in tumorigenesis [16]. PTP1B deactivates oncogenes or tumor suppressors to act as a tumor promoter in

various cancers, including colorectal cancer, non-small cell lung cancer, hepatocellular carcinoma, and gastric cancer [17]. PTP1B has been implicated in the oncogenesis of breast cancer and treatment with a PTP1B inhibitor greatly slowed down the growth of breast tumors [18] which courageously results into MSI-1436C, this is an anti-diabetic lead candidate is being tested against metastatic breast cancer under Phase 1 trials [19]. PTP1B, a viable target for cardiovascular diseases. PTP1B is specifically prominent in endothelial cells, where it might play a part in endothelial dysfunction. Also, inhibition of PTP1B has a tendency to downregulate cardiac angiogenesis by negative regulation of Vascular endothelial growth factor (VEGF) signaling. Not only in the context of metabolic illnesses, but also in the situation of heart failure, inhibiting PTP1B has positive effects on cardiac dysfunction and remodeling as a result of its endothelium protecting and/or proangiogenic actions. Therefore, this enzyme offers a tempting new therapeutic target for treatment of cardiovascular disorders as well.

According to available structural data of PTP1B enzyme, the active region in the protein can be divided into five sub pockets, (A, B, C, D, and E) out of which three major sites, A, B and C are imperative for protein function and to control insulin signaling pathways (Fig. 1A) [20, 21]. The insulin receptor (IR) kinase activation peptide's phosphotyrosine (pTyr) residues were dephosphorylated at the primary phosphate-binding pocket [22] known as A site which is of 10Å in width and 9Å in length consists of Cys215, Gln262, Gln266 and Arg221 residues [23, 24]. The secondary binding pocket B site where side chain of pTyr is bound includes Val49, Met258, Arg254, Phe52, Arg24, Gly259, and Ile219 forming a shallow and non-catalytic region but important for improving action and selection of small molecules. The third site C is large, flat and also known as third phosphate binding pocket which can be occupied by negatively charged groups present in amino acids Asp48, Lys41, Arg47, and Tyr46 [25, 26]. Various potent inhibitors reported till date are specifically developed to bind at C site such as carboxylates [23, 27], phosphonates [28, 29], cinnamates [30, 31] or malonates [32, 33] but they are either bulky, lipophilic or negatively charged making their physicochemical properties incapable for bioavailability [34]. These inhibitors could be categorized broadly into two types: competitive and noncompetitive inhibitors [35, 36]. Crystallographic studies have shown that non-competitive inhibitors bind at an allosteric site which is at a distance of 20 Å from the catalytic site and molecules from different chemical moieties like benzofuran/benzothiophene biphenyl oxo-acetic acids (A) [37], 11-arylbenzo[b]naphtho[2,3- d]furans/thiophenes (B) derivatives [38], and benzofuran-cored compounds (C) [36] have been reported to bind non-competitively (Fig. 1B).

In a continuous effort to identify novel PTP1B inhibitors [39–41], the present work made use of ligand based and structure-based approach in combination to find hit molecules against target enzyme PTP1B (Fig. 2). Initially, pharmacophore modelling was performed to find common features like two hydrogen bond acceptors, an aromatic ring and one hydrogen bond donor from the ligands with reported inhibition activity against PTP1B. The dataset of compounds with common pharmacophoric feature were filtered to remove pains substructure and to retain drug likeness. Then with the application of molecular docking and molecular dynamic simulations followed by binding free energy calculations i.e. MM_PBSA new hits were found to target PTP1B.

2. Results And Discussion

2.1 Pharmacophore-based virtual screening

Based upon the inhibition activity of five different ligands perceived from Binding DB web-server [42], their co-crystalized 3D structures with PTP1B protein were downloaded and with the help of PyMOL software [43] the ligand structures were extracted. On submission to Pharmit web application [44], these five ligands were found to have various common pharmacophoric features such as two negative ions (N1 and N2), one hydrogen donor (HD), five hydrogen acceptor (HA1, HA2, HA3, HA4 and HA5) and one aromatic (A) feature as represented in Fig. 3A. For obtaining optimum quantity of compounds for structure-based screening, we excluded some of these features viz. two negative ions, three hydrogen acceptor which were constraining the number of query results and used only four inclusive features (HA1, HA5, A and HD)

consisting of one hydrogen donor, one aromatic and two hydrogen acceptors as depicted in Fig. 3B. The pharmacophoric screening resulted into 18887 molecules retaining query features with RMSD lower than 0.5 Å from Mcule-Ultimate database containing 126,471,502 molecules. The interatomic distances between each of the pharmacophoric feature is presented in Table 1, which was calculated using measurement wizard of the PyMOL software.

Table 1
Measure of relative distances between different pharmacophoric features

Pharmacophoric features	A	N1	N2	HA1	HA2	HA3	HA4	HA5	HD
A	-	3.0	5.4	3.7	3.8	4.0	6.0	6.1	10.4
N1		-	4.7	1.2	1.2	3.1	5.0	5.8	11.8
N2		4.7	-	5.9	3.9	2.4	1.2	1.2	10.5
HA1	3.7	1.2	5.9	-	2.0	4.1	6.1	6.9	12.7
HA2	3.8	1.2	3.9	2.0	-	2.7	4.0	5.0	11.7
HA3	4.0	3.1	2.4	4.1	2.7	-	3.2	3.0	11.8
HA4	6.0	5.0	1.2	6.1	4.0	3.2	-	2.1	10.8
HA5	6.1	5.8	1.2	6.9	5.0	3.0	2.1	-	10.4
HD	10.4	11.8	10.5	12.7	11.7	11.8	10.8	10.4	-

2.2 PAINS and Drug likeness filter

An RDKit-based KNIME workflow [45, 46] was prepared and used for Pan Assay Interference Compounds (PAINS) filtering of compounds obtained from pharmacophore-based screening where the PAINS like fragments and functional groups were converted into SMARTS (SMILES arbitrary target specification) pattern. Then, all the ligands were examined for presence of these SMARTS pattern and found 316 compounds were with matching pattern were filtered out. We got 18571 molecules which were further checked for finding any molecule violating Lipinski Rule of Five (MW < 500, HDonor < 5, HAcceptor < 10, LogP < 5, Rotatable bods < 10). Out of 18571, we selected 5867 molecules which do not violate any of the rule from Lipinski. Finally, in order to enrich the set of compounds with structural diversity, we applied RDKit Diversity Picker and choses 1500 molecules. From this set, molecules already reported with PTP1B inhibition were also removed to get a final data set of 1484 molecules.

2.3 Ligand, Protein Preparation and Validation

Ligands and receptor structures were prepared using Open Babel [47] and MGL Tools [48]respectively. For validation of grid and docking, the co-crystalized ligand was redocked into the binding site of PTP1B enzyme. We found that the co-crystalized ligand which binds to deep cavity overlaps with RMSD 1.19 Å, a little higher that might be due to the presence of rotatable bonds at central portion of the ligand but RMSD value is within the acceptable limit (Fig. 4A). We used Ertiprotafib as a control/standard molecule that is a reported inhibitor of PTP1B enzyme that reached clinical trials but failed due to its side effects [49]. We performed its docking and redocking in the same grid and found that it was showing lower RMSD value that is 0.07 Å (Fig. 4B). Therefore, superimposition of the docked structures suggested that the generated grid is correct.

2.4 Structural-based virtual screening

The prepared ligands along with standard i.e. Ertiprotafib were used for virtual screening which was carried out using AutoDock Vina software [50] under flexible ligand mode. The binding score of molecules varies from − 6.3 to -10.5 kcal/mol for 1487 molecules and output file contained 5–8 poses of each ligand. Top fifty molecules were selected out of

these 1484 based upon the binding score ranging from − 10.5 to 9.3 kcal/mol. The first pose of top fifty molecules was extracted and saved in SDF format for ADME (absorption, distribution, metabolism, and excretion) prediction. The 2D structures of Ertiprotafib and top ten hits are presented in the Fig. 5.

Then the top five compounds with good pharmacokinetic properties like high absorption, solubility and permeability were chosen further for performing molecular dynamics study. The 2D and 3D interaction diagram of the top five compounds and Ertiprotafib with PTP1B enzyme are presented in Figs. 6 and 7. Coming to interaction of docked poses, **Ertiprotafib** showed various interactions such as carbonyl oxygen was forming hydrogen bonding with LYS120 & SER216; benzyl and phenyl ring forming π-π stacking with PHE182; and ALA217 & VAL49 are interacting with phenyl & methyl groups via alkyl & π-alkyl bonding. TYR46 residue was found to be interacting through π-σ interaction with methyl group present at phenyl ring; ASP48 has shown π-anion interaction with naphtho-thiophene ring holding a score of -9.3 kcal/mol (Fig. 6A **& B**). Subsequently, **Compound M4** has docking score of -10 kcal/mol and showed several hydrogen bonds such as oxazole ring with ARG221 & PHE182; carbonyl groups attached to quinazolinone & naphthyridinone with VAL120; carbonyl group present at bridge with ARG221. It also showed π-π interaction between quinazolinone and TYR46 & PHE182; π-alkyl bonding of quinazolinone with ALA217 and last but not least, it also demonstrated π -anion and π-alkyl interaction of LYS116 with naphthyridinone ring (Fig. 6C **& D**). **Compound M5** displayed binding affinity of -9.5 and represented hydrogen bond and π-alkyl interaction of LYS116 with fluorine and oxadiazole ring. Likewise, compound M4, ARG221 showed two hydrogen bonds with both phenol and tetrazole ring and one π-alkyl interaction with tetrazole ring. Apart from these conventional interactions it is also stabilized by π-anion interaction with LYS120; pi-donor hydrogen bond between pyridine & SER118, tetrazole & PHE182 and pyrrolidine & ASP181. Furthermore, π-π stacking and π-alkyl interaction of phenyl ring with TYR46 and ALA217, respectively was also observed for this compound (Fig. 6E **& F**). **Compound M6** which showed docking score of -9.8 kcal/mol and was forming two hydrogen bonds between nitrogen & carbonyl oxygen of tetrahydro-quinazolinone ring and ALA217 & ARG221 respectively; one π-anion interaction between ASP48 and phenyl ring; π-donor hydrogen bond between tetrahydro-quinazolinone and SER216. Additionally, it was also stabilized through several π-alkyl interactions between cyclopentane and ALA27 & MET258; piperazine and MET258; tetrahydro-quinazolinone and PHE182, TYR4, CYS215 & ALA217 (Fig. 7A **&B**). Analogous to other compounds, **Compound M8** with the binding affinity of -9.8 kcal/mol, displayed hydrogen bonding interactions like ARG221 with tetrazole; Fluorine with ARG24 and carbonyl with ARG254. The tetrazole moiety of M8 showed π-anion interaction CYS215 & ARG221 and π-π stacking interaction with PHE182 residue. In addition, two π-alkyl interaction were observed by the ALA27 residue with terminal phenyl ring and ALA217 & ILE219 with central phenyl ring (Fig. 7C **&D**).

Compound M9 presented in Fig. 7**(E & F)** shown a binding score of -9.4 kcal/mol and interacted through one hydrogen bond between pyrimidinedione and ARG254, and one π-π interaction between TYR46 and pyrrolo-pyridine. It was also found to be stabilized through non-conventional bonds such as π-donor hydrogen interaction of methyl group with GLU115 & ASP181 and GLN262 with pyrimidinedione ring; π-alkyl interaction of pyrrolo-pyridine with various amino acids like LYS120, ALA217, PHE182 & TYR46 and lastly π-sigma interaction between tert-butyl and PHE182 residue.

Therefore, interactions of compounds with PTP1B highlighted that hydrogen bonding and π- π interactions were playing significant role in binding process. Non-conventional interactions like π-alkyl, π-anion and π-donor hydrogen were also displayed by the molecules helping for their stabilization inside the binding pocket of PTP1B enzyme. The compounds M4, M5, M6 and M8 were clearly seen to bind with the residues present in A site of the PTP1B enzyme which is important and play a key role in catalysis. On the other hand, compound M9 bind to the B-site which is a secondary site for catalysis while Ertiprotafib bound at C site that is an imperative site for selectivity.

2.5 ADME Predictions

The pharmacokinetic properties of Ertiprotafib and top fifty compounds were predicted with the help of DruMAP online web server (https://drumap.nibiohn.go.jp/prediction) that can be freely accessible and data of ten compounds with that of

standard is presented in the Table 2. Various parameters including drug metabolism were calculated such as solubility (d_sol74), fraction of human intestinal absorption (*fa_human*), permeability measured using caco-2 cell line (*papp_human_caco2*) [51], brain-to-plasma concentration ratio (*Kp_brain*), unbound brain-to-plasma concentration ratio ($K_{p,uu,brain}$) [52], fraction of drug excreted unchanged in the urine (f_e), predicted fraction unbound in plasma ($f_{u,p}$) [53] and renal clearance (CL_r) [54]. Since solubility, absorption and permeability are the major parameters that may cause the drug failure at initial stages, so we have selected only those compounds which showed high value for these three parameters i.e. sol > 100µL, fa > 0.7 and Papp > 10^{-5}cm/s) for further studies highlighted in Table 2.

Table 2
Pharmacokinetic Properties of the top 10 molecules along with their docking score predicted by DruMAP

Compound Name	Dock score	fa_ human	papp_ human caco2	d_sol 74	fe_ human	clr_ human	fu_p_ human class	fu_p_ human value	kp_ brain	kp_uubrain
Ertiprotafib	-9.3	Moderate	Low	Low	Low	0.0054	Low	0.0076	2.827	4.771
M1	-10.5	Moderate	Low	Low	Low	0.0610	High	0.1744	0.034	0.014
M2	-9.3	High	High	High	Low	0.0459	High	0.1154	0.014	0.016
M3	-9.3	High	High	High	Low	0.0585	High	0.1222	0.211	0.503
M4	**-10**	**High**	**High**	**High**	**Low**	**0.0385**	**High**	**0.0988**	**0.072**	**0.223**
M5	**-9.5**	**High**	**High**	**High**	**Low**	**0.0413**	**High**	**0.0997**	**0.066**	**0.036**
M6	**-9.8**	**High**	**High**	**High**	**Low**	**0.0488**	**High**	**0.1964**	**0.737**	**0.282**
M5	-9.3	High	High	High	Low	0.0380	Low	0.0727	0.064	0.116
M8	**-9.8**	**High**	**High**	**High**	**Low**	**0.0310**	**Low**	**0.0715**	**0.027**	**0.055**
M9	**-9.4**	**High**	**High**	**High**	**High/ Medium**	**0.0693**	**High**	**0.1644**	**< 0.01**	**0.031**
M10	-9.4	High	High	High	Low	0.0376	Low	0.0467	1.740	2.205

fa_human: fraction of human intestinal absorption; papp_human_caco2: permeability measured using caco-2 cell line; Kp_brain: brain-to plasma concentration ratio; $K_{p,uu,}$brain: unbound brain-to-plasma concentration ratio; $f_{e_}$human: fraction of drug excreted unchanged in the urine; $f_{u,p}$: predicted fraction unbound in plasma; CL_r: renal clearance and d_sol74: solubility .

2.6 Molecular Dynamics Trajectory Analysis

Top five compounds which were having high solubility, absorption and brain permeability were selected further for evaluation of ligand stability inside the binding site of PTP1B using classical all-atom molecular dynamics simulation study. Docked pose of top ligands with protein structure after virtual screening via Autodock vina [50] was used for simulation study of 100 ns using GROMACS 2020 [55].

The Root Mean Square Deviation (RMSD) was used to measure the average change in displacement of a selected atoms for a particular frame relative to atoms of reference frame. Monitoring the RMSD of the complex can provide information about changes in its structural conformation throughout the simulation. The RMSD plot depicts (Fig. 8A) that **Ertiprotafib** and **Complex M5** have been stabilized with equivalent and lowest value of ~ 0.2nm on an average among all of the complexes. Similarly, average RMSD value for **Complex M4** and **Complex M8** was found to be ~ 0.28nm. These results strongly suggested that all these complexes are stable since their RMSD values were stabilized around a fixed value.

However, the **Complex M6** and **M9** have highest RMSD value swapping between 0.3–0.9 nm, which is not acceptable and indicating that the system is not stabilized at all. The radius of gyration was also measured throughout the time period of simulation to characterize the compactness of the protein structure in the presence of ligand. Four complexes namely **Complex M4, M5, M8** and **Ertiprotafib** exhibited a similar pattern of radius of gyration in between 0.94–0.97 nm during the simulation (Fig. 8B). On the other hand, **Complex M6** and **M9** is showing large variation in the plot fluctuating in between 0.2–2.14 nm. In order to measure local changes and individual residue flexibility along the protein chain during the simulation time period, RMSF was determined. Overall RMSF value for all six complexes remained within the range of 0.05–1.5 nm for the entire simulation period (Fig. 9A). Higher fluctuations can be observed for various residues present in the loop regions such as 30–38, 52–60, 127–140, 180–190, 202–215 and 235–240 among terminal residues. Highest RMSF value was observed for protein complexed with **Compound M9**. Ligand RMSF values were also measured presented in the Fig. 9C **Ertiprotafib** and **Compound M4** has lower RMSF value of 0.025-0.2 nm than other compounds except for last 3–4 atoms of **Ertiprotafib** which were having RMSF of 0.2–0.3 nm. For other ligands such as **M5, M6, M8** and **M9** the RMSF value is changing from 0.025–0.35 nm. Fluctuations in the ligand are indicative of small structure of molecules trying to stabilize in the binding site of the protein. Since formation of hydrogen bonds play a significant role in ligand binding and stability of the complex, number of hydrogen bond formed during simulation was also calculated. The results of hydrogen bond formed between protein and ligand are presented in the Fig. 9B. It can be clearly seen from the h-bond plot that the **Compound M4, M5** and **M8** are forming at least 2 3 and 5 hydrogen bond throughput the simulation depicting that hydrogen bond formation has vital role in stabilization of these compounds in the binding site of the protein. While **Ertiprotafib, Compound M6** and **M9** are having less than 30% of hydrogen bond occupancy for whole simulation time period signifying that there is less chance of hydrogen bonds to be involve in the stabilization of complex formation. Finally, Fig. 9D displayed hydrogen bond length distribution throughout the trajectory showing that all the hydrogen bonds formed were within the cut off value of 0.35nm.

Free energy landscape (FEL) is mapping of all possible conformations that a molecule undergoes during a simulation to the corresponding energy. It shows the complex undergoing valleys and mounds of free energy and helps to represents the structure having lowest energy [56]. It is calculated by using sham command provided by Gromacs tool [57] in terms of two variables that replicate specific properties of the system and characterize conformational changes, for example here we have used RMSD and radius of gyration. The third variable is the free energy, which can be estimated from the distribution (probability distribution) of the system relative to the previously selected variable. In 3D representation, the shape and valleys in the topography represent low free energy regions (blue), representing the metastable conformations of the system, and the hills represent the energy barriers connecting these metastable states (dark red).

Figure 10 and 11 revealed the changes in Gibbs free energy (ΔG) values for **Ertiprotafib, Complex M4, M5, M6, M8** and **M9** having a range between 0–10, 0-9.35, 0-9.9, 0-11.7, 0–9 and 0-9.8 kJ/mol respectively. If we precisely observe the 2D and 3D contour of **Ertiprotafib, Complex M4, M5** and **M6** it clearly depicts that these complexes possess only one valley which means there is no transition barrier on the surface of a single well to reach local energy-minima with one stable folding state throughout the simulation. While the **Complex M8** and **M9** have two local energy minima with one major conformation out of two slightly different geometrical conformations that was attained by the complex to attain the global energy minima but they both seems to lie very close within the 3D space as seen in the graph and is having a relatively stable folding process. FEL of **Compound M6** and **M9** were observed to be in a very brief blue region suggesting their instability and higher energy. Overall, MD results indicated that **Compound M4, M5** and **M8** are having good binding affinity with higher number of interactions and lower RMSD value throughout the simulation while **Compound M6** and **M9** were highly unstable and were found to be detached from the active site of PTP1B enzyme many a times throughout the simulation in trajectory visualization.

Subsequently, from free energy landscape profile the coordinates of three stable complexes with lowest energy that is 0 kcal/mol were noted down and these coordinates were used to extract the frame corresponding to energy minima. We tried

to overlap the docked complex over the lowest free energy-minima structure to see the differences in binding pose of ligands and the results are displayed in Fig. 12 along with 2D interactions of the FEL extracted frame. The local minima structure of **Ertiprotafib** corresponded to the rGy and RMSD (1.95773, 0.22908) when overlapped with the docked pose, RMSD value of the complex was found to be 1.226Å. 3D representation of the same revealed that conformation of Ertiprotafib is much varied and phenyl group fit inside the binding pocket while naphtho-thiophene ring lie outside. It is interacted with PHE182, TYR20, ASP48, VAL49, GLN262 and LYS116 through various bonds like pi-pi stacking, pi-alkyl, pi-anion, pi-donor hydrogen bonds. It lacks the hydrogen bonds as seen in docked pose matching with the MD results. When the local minima structure of **Compound M4** corresponds to rGy and RMSD (1.95985, 0.24689), aligned with the docked pose, RMSD value of the complex was found to be 1.450Å. The conformation of **Compound M4** is little varied though showing similar binding pose as well as interactions where oxazole is fitted into the cavity and naphthyridinone ring lying outside. It displays three hydrogen bonds with ASP181, ARG221 & LYS116 and two pi-pi interaction with TYR46 & PHE182. On alignment of local minima structure of **Compound M5** corresponds to rGy & RMSD (1.94677, 0.20333), with the docked pose, RMSD value of the complex was found to be 1.185Å. The conformation of Compound M5 was changed but a similar binding pose was found to be with tetrazole fitted inside the cavity and pyridine ring lying outside. The local minima structure of **Compound M8** corresponds to rGy and RMSD (1.95106, 0.26197), when overlapped with the docked pose, RMSD value of the complex was found to be 1.022Å. The conformation of **Compound M8** also varied before and after MD but, in both conformations, tetrazole fitted inside the cavity and other part of the ligand are interacting at different sites. It is displaying several hydrogen bonds with many amino acids such as ARG221, ASP181, GLN262, ARG47, GLY220, ALA217 & GLY218; halogen bonding through ARG45, pi-pi stacking with TYR46; pi-alkyl interaction with ILE219, ALA217 and also interacts with TYR46 by forming pi-donor hydrogen bond.

2.7 Molecular mechanics Poisson–Boltzmann surface area (MM_PBSA) Analysis

To estimate the molecular binding interaction of the top five hits and Ertiprotafib at the binding pocket of PTP1B protein, we determined the binding free energy (ΔG) using MM-PBSA approach as represented in the violin plot (Fig. 13). These calculations involve the energetic terms that is accounted for van der Waals contribution from molecular mechanics, the electrostatic contribution in terms of electrostatic energy to the solvation free energy which is calculated by generalized Born, and nonpolar contribution to the solvation free energy calculated by an empirical model. To assess the binding free energy throughout the simulation, we primarily performed MM-PBSA calculation on the lowest energy minima frame of the simulation trajectory and two of its adjacent frames, the resultant ΔG was then taken as an average of the three frames (Table 3). Furthermore, the individual component contribution for the binding can be seen as the van der Waals and surface energy has positively contributed to the overall binding interaction in all the complexes (Fig. 14).

The electrostatic contribution has positive contribution for all complexes except **M5** and **M8**. EGB and solvation energy both has negative contribution for all complexes except for **Complex M5** and **M8**. While GGAS energy has positive contribution for all complexes except **Complex M8**. Conclusively the total binding free energy for all the complexes were having negative value. Supporting MD results, binding free energy also displayed that the **Compound M4, M5** and **M8** were found to have better binding affinity for PTP1B enzyme with ΔG_{total} score of -24.25, -31.47 and − 33.81 kcal/mol respectively as compared to other compounds.

Table 3
MM-PBSA binding free energy (ΔG) calculations for Ertiprotafib and top 5 hits with PTP1B protein

Complex	Van der Waals	Electrostatic energy	EGB	ESURF	GGAS	GSOLV	Averaged ΔG (kcal/mol)
Ertiprotafib	-32.53	-11.38	27.65	-4.65	-43.91	23	-20.91
Complex M4	-29.4	-25.24	34.6	-4.2	-54.65	30.39	-24.25
Complex M5	-31.01	8.78	-5.72	-3.52	-22.23	-9.24	-31.47
Complex M6	-16.01	7.5	2.2	-2.02	-8.52	0.18	-8.34
Complex M8	-30.89	44.24	-43.78	-3.37	13.35	-47.15	-33.81
Complex M9	-28.1	-14.68	30.79	-3.47	-42.79	27.32	-15.47

EGB = the electrostatic contribution to the solvation free energy calculated by PB or GB; ESURF = nonpolar contribution to the solvation free energy calculated by an empirical model; GGAS = Gibbs free energy into a gas-phase term; GSOLV = Gibbs free energy into a solvation term.

3. Materials And Computational Methods

3.1 Mapping of pharmacophoric features and development of pharmacophore

Five compounds complexed with PTP1B were chosen from Binding DB a database [42], based on the Ki value less than 100 nM for these compounds. The crystal structures of these selected complexes were downloaded from Protein Data Bank (PDB) [58] holding PDB IDs (2CNE [59], 2QBP [60], 1NNY [61], 1NZ7 [62] and 2QBQ [63]). The ligands from these PDB IDs were extracted with the help of PyMOL v4.6.0 [43] where amino acid chain was removed and 3D structures of the ligands were saved in mol2 format. These five structures were used to generate pharmacophore model using freely accessible webserver PharmaGist [64] (http://bioinfo3d.cs.tau.ac.il/PharmaGist/php.php) bearing common pharmacophoric features.

3.2 Pharmacophore based virtual screening

The best pharmacophore model obtained was employed as a query to screen Mcule-Ultimate (https://ultimate.mcule.com/) database having 378,803,44 conformers of 126,471,502 molecules using Pharmit server [44]. The query results contain a set of 18887 molecules which were further used for structure based virtual screening. The obtained molecules were a result of process involving superimposition of molecules against the pharmacophore to minimize RMSD between the queried features and hit compounds.

3.3 PAINS and Drug likeness filter

PAINS are chemical compounds which frequently produce false positive results in high-throughput screening. Typically, PAINS binds non-specifically with more than one biological target rather than binding to one intended target specifically. Thus, prior to virtual screening the molecules were filtered to remove PAINS substructure using RDkit [45] molecule catalog filter to obtain 18571 molecules. Subsequently, drug likeness filter was also applied to remove compounds violating Lipinski's Rule of Five (i.e., MW < 500 Da, ≤ 5 hydrogen bond donors, ≤ 10 hydrogen bond acceptors, and an octanol–water partition coefficient log P ≤ 5) resulting in a set of 5867 molecules. Then, RDKit Diversity picker was used to pick

1500 diverse molecules free from duplicates. All these filters were applied using an open-source application KNIME analytics platform (ver. 4.3.2) [46, 47], that uses numerous knime nodes including SDF reader, RDKit Molecule Catalog Filter, Lipinski's Rule-of-Five, RDKit Diversity Picker and SDF writer. The molecules were further screened to remove any molecules already reported in Binding DB, to get final set of 1484 compounds for docking studies.

3.4 Structure based Screening

3.4.1 System Preparation

The selected molecules obtained were in SDF format and using Open Babel 3.1.1 [47] their geometry was optimized followed by energy minimization and conversion into PDBQT format. The protein structure (PDB ID 2CNE) was prepared using MGL Tools v1.5.6 [48] in which polar hydrogen and Kalman charges were added, atoms were assigned AD4 type and finally protein structure was saved in PDBQT format.

3.4.2 Grid generation and Validation of molecular docking

With the help of AutoDock utility Grid, a grid box of size 30*30*30 Å with center 17.699*30.224*18.544 (in x, y and z direction respectively) was formed around the binding pocket where the co-crystalized ligand was bound/placed. To validate the grid, the co-crystalized ligand and standard i.e., Ertiprotafib were redocked. Before performing actual screening, we examined the RMSD values between the redocked and experimentally determined co-crystallized ligand using PyMOL. RMSD is widely used for quantitative measurement of the similarity between two superimposed molecules. RMSD values are measured in angstrom and calculated by the following equation.

$$RMSD = \sqrt{\frac{1}{n}\sum_{i=1}^{n} d_i^2}$$

Where the averaging is done across n pairs of similar atoms and d i denotes the distance between the two atoms in i^{th} pair. RMSD parameter required is not more than 1.5 Å to conclude that the protocol used was valid and this could be put to use in the docking procedure.

3.5 Molecular Docking/Virtual screening

Vina application [50] was used for performing virtual screening and exhaustiveness value was kept eight for molecular docking cum virtual screening. Virtual screening was performed using a perl script which helps to execute docking of large number of compounds in a run which take configuration file, ligand name file, receptor structure in pdbqt format and ligand structure in pdbqt format. After docking studies, the first model/structure from each ligand was extracted and saved in a same file. And top 50 compounds with high binding affinity (more negative score) were selected further for ADME studies.

3.6 In silico ADME prediction

ADME properties are assessed using in silico tools which helps in filtering such molecules consist of poor pharmacokinetic properties, that is an essential part of drug discovery since it led to failure of drugs in clinical trials. We used DruMAP v1.4 (Drug Metabolism and Pharmacokinetics Analysis Platform) for prediction of DMPK parameters such as solubility, clearance [54], absorption, cell permeability [51], BBB permeability [52] where structure of molecules were uploaded in sdf format (https://drumap.nibiohn.go.jp/).

3.7 Molecular Dynamics Simulation

The compounds which showed better activity were chosen to perform MD simulation for 100 ns with GROMACS 2020 [55] as described in various literatures [65, 66]. Briefly, the system was built using CHARMM-GUI webserver using CHARMM-

36M as force field [67]. The protein was solvated using TIP3P water model to accommodate a rectangular box of dimensions 14.08x13.57x13.86 nm, and neutralized by using Monte Carlo ion placing method, adding Na^+ and Cl^- ions. The energy of the neutralized system was minimized in 50,000 steps using the steepest descent algorithm followed by equilibration for a time period of 1 ns using the NVT ensemble, by restraining the protein. The temperature was kept constant at 303.15 K with Noose Hoover thermostat [68] and a coupling constant of 1.0 ps was applied for both the protein and nonprotein atoms. Then, the system was equilibrated using NPT ensemble for a time period of 1 ns at 1 bar pressure using the Parrinello-Rahman barostat [69] with a coupling constant of 1 ps. At last, the system was subjected to isobaric-isothermal ensembled MD production simulation for 100 ns. In the meantime, the time step was set at 2 fs throughout the simulation. LINCS (LINear Constraint Solver) algorithm was used for the bond's length constraints. Particle mesh Ewald (PME) strategy was adopted for long-range electrostatic interactions, with a cut-off radius of 1.2 nm and 0.16 nm grid spacing. The cut-off distance for Van der Waals was set to 1.2 nm. After completion of production run the trajectories were analyzed for root mean square deviation (RMSD), root mean square fluctuations (RMSF), radius of gyration (rGy) and free energy landscape with the help of GROMACS.

3.7 MM-PBSA calculation

The coordinates of energy minima structure and its two neighboring frames of the trajectory were obtained from the Free Energy Landscape diagram. For the calculations of gmx_MMPBSA, we have used single trajectory approach to calculate the binding free energy differences. gmx_MMPBSA [70] is a tool scripted in Python3.8 that integrate the functionality from AmberTools and GROMACS in order to build input files in an accurate method that can be reproducible so as to perform the end-state free energy calculations. The work have been carried out in three crucial steps (i) preparation where the MMPBSA.py calculation engine provided in the gmx_MMPBSA was used to carry out the calculations, the md simulation output topology files from GROMACS was used for conversion into Amber topology format, (ii) multiple calculations are carried out for binding free energy with different solvation models (PB, GB, or 3D-RISM), and (iii) visualization and analysis was performed once the calculations are complete by using graphical user interface application (gmx_MMPBSA_ana), which helps to view and analyze the data.

4. Conclusion

In this work, a rational approach was accomplished by means of ligand-based screening followed by structure-based screening to find potential hit compound as inhibitors of PTP1B protein. We designed a pharmacophore model based upon such ligands reported to have inhibition activity against PTP1B protein which were filtered for drug likeness and PAINS substructures. Resultant dataset was docked against PTP1B protein to find hit molecules with good binding score. Then physicochemical properties were calculated for top fifty compounds which were having good binding score against PTP1B protein. The compounds with optimum value of absorption, solubility and permeability were selected further for simulation studies. The molecular simulation studies analyzed important interactions and conformational stability and integrity of the protein-ligand complexes. Based upon MD simulations we have found three molecules Compound M4, M5 and M8 were showing best results with effectively stabilized complex among all other compounds. These compounds showed various interaction like hydrogen bond formation and pi-stacking which favored the attachment of these ligands with the receptor. Further compound M6 and M9 were having destabilizing effect on the protein during simulation and they were detached from the binding pocket and were found to have lesser number of hydrogen bonding throughout the simulation.

The analysis of average binding free energy and the individual energy components showed the stability of all the complexes. The overall results from the molecular dynamics and binding free energy both displayed that the compound M4, M5 and M8 were having better binding affinity for PTP1B enzyme with ΔG_{total} score of -24.25, -31.47 and − 33.81 kcal/mol respectively than other compounds. The results of this in silico approach revealed that the combined ligand and structure-based screening can help in better way to find a suitable lead molecule.

Declarations

Acknowledgement

Dr. Rajnish Kumar is grateful to the Indian Institute of Technology (BHU) Varanasi for the seed grant and Science Engineering & Research Board (SERB), India for providing start-up research grant (SRG/2021/000415). Bharti Devi is grateful to SERB for providing Junior Research Fellowship. The support and the resources provided by 'PARAM Shivay Facility' under the National Supercomputing Mission, Government of India at the Indian Institute of Technology (BHU), Varanasi are gratefully acknowledged.

References

1. R.N. Shinde, G.S. Kumar, S. Eqbal, M.E. Sobhia, Screening and identification of potential PTP1B allosteric inhibitors using in silico and in vitro approaches, PloS one, 13 (2018) e0199020.
2. N.K. Tonks, Protein tyrosine phosphatases–from housekeeping enzymes to master regulators of signal transduction, The FEBS journal, 280 (2013) 346–378.
3. W.J. Hendriks, A. Elson, S. Harroch, R. Pulido, A. Stoker, J. den Hertog, Protein tyrosine phosphatases in health and disease, The FEBS journal, 280 (2013) 708–730.
4. A. Alonso, J. Sasin, N. Bottini, I. Friedberg, I. Friedberg, A. Osterman, A. Godzik, T. Hunter, J. Dixon, T. Mustelin, Protein tyrosine phosphatases in the human genome, Cell, 117 (2004) 699–711.
5. D. Barford, Molecular mechanisms of theprotein serine/threonine phosphatases, Trends in biochemical sciences, 21 (1996) 407–412.
6. M.T. Ha, D.H. Park, S. Shrestha, M. Kim, J.A. Kim, M.H. Woo, J.S. Choi, B.S. Min, PTP1B inhibitory activity and molecular docking analysis of stilbene derivatives from the rhizomes of Rheum undulatum L, Fitoterapia, 131 (2018) 119–126.
7. X. Zhang, H. Jiang, W. Li, J. Wang, M. Cheng, Computational insight into protein tyrosine phosphatase 1b inhibition: a case study of the combined ligand-and structure-based approach, Computational and mathematical methods in medicine, 2017 (2017).
8. T.O. Johnson, J. Ermolieff, M.R. Jirousek, Protein tyrosine phosphatase 1B inhibitors for diabetes, Nature Reviews Drug Discovery, 1 (2002) 696–709.
9. F. Ahmad, J.L. Azevedo, R. Cortright, G.L. Dohm, B.J. Goldstein, Alterations in skeletal muscle protein-tyrosine phosphatase activity and expression in insulin-resistant human obesity and diabetes, The Journal of Clinical Investigation, 100 (1997) 449–458.
10. P.S. Rao, C. Muvva, K. Geethanjali, S.B. Bastipati, R. Kalashikam, Molecular docking and virtual screening for novel protein tyrosine phosphatase 1B (PTP1B) inhibitors, Bioinformation, 8 (2012) 834.
11. H.Y. Hsing, S. Rathnasamy, R. Dianita, H.A. Wahab, Docking-based virtual screening in search for natural PTP1B inhibitors in treating type-2 diabetes mellitus and obesity, Biomedical Research and Therapy, 7 (2020) 3579–3592.
12. M.N. Vieira, N.M. Lyra e Silva, S.T. Ferreira, F.G. De Felice, Protein tyrosine phosphatase 1B (PTP1B): a potential target for Alzheimer's therapy?, Frontiers in Aging Neuroscience, 9 (2017) 7.
13. M. Elchebly, P. Payette, E. Michaliszyn, W. Cromlish, S. Collins, A.L. Loy, D. Normandin, A. Cheng, J. Himms-Hagen, C.-C. Chan, Increased insulin sensitivity and obesity resistance in mice lacking the protein tyrosine phosphatase-1B gene, Science, 283 (1999) 1544–1548.
14. A. Cheng, N. Uetani, P.D. Simoncic, V.P. Chaubey, A. Lee-Loy, C.J. McGlade, B.P. Kennedy, M.L. Tremblay, Attenuation of leptin action and regulation of obesity by protein tyrosine phosphatase 1B, Developmental cell, 2 (2002) 497–503.

15. J.M. Zabolotny, K.K. Bence-Hanulec, A. Stricker-Krongrad, F. Haj, Y. Wang, Y. Minokoshi, Y.-B. Kim, J.K. Elmquist, L.A. Tartaglia, B.B. Kahn, PTP1B regulates leptin signal transduction in vivo, Developmental cell, 2 (2002) 489–495.
16. L. Lessard, M. Stuible, M.L. Tremblay, The two faces of PTP1B in cancer, Biochimica et Biophysica Acta (BBA)-Proteins and Proteomics, 1804 (2010) 613–619.
17. L.R. Bollu, A. Mazumdar, M.I. Savage, P.H. Brown, Molecular Pathways: Targeting Protein Tyrosine Phosphatases in CancerTargeting Protein Tyrosine Phosphatases in Cancer, Clinical Cancer Research, 23 (2017) 2136–2142.
18. L.E. Arias-Romero, S. Saha, O. Villamar-Cruz, S.-C. Yip, S.P. Ethier, Z.-Y. Zhang, J. Chernoff, Activation of Src by protein tyrosine phosphatase 1B Is required for ErbB2 transformation of human breast epithelial cells, Cancer research, 69 (2009) 4582–4588.
19. Q. Xu, N. Wu, X. Li, C. Guo, C. Li, B. Jiang, H. Wang, D. Shi, Inhibition of PTP1B blocks pancreatic cancer progression by targeting the PKM2/AMPK/mTOC1 pathway, Cell death & disease, 10 (2019) 1–15.
20. A. Salmeen, J.N. Andersen, M.P. Myers, N.K. Tonks, D. Barford, Molecular basis for the dephosphorylation of the activation segment of the insulin receptor by protein tyrosine phosphatase 1B, Molecular cell, 6 (2000) 1401–1412.
21. Z. Jia, D. Barford, A.J. Flint, N.K. Tonks, Structural basis for phosphotyrosine peptide recognition by protein tyrosine phosphatase 1B, Science, 268 (1995) 1754–1758.
22. X. Li, L. Wang, D. Shi, The design strategy of selective PTP1B inhibitors over TCPTP, Bioorganic & Medicinal Chemistry, 24 (2016) 3343–3352.
23. J.N. Andersen, O.H. Mortensen, G.n.H. Peters, P.G. Drake, L.F. Iversen, O.H. Olsen, P.G. Jansen, H.S. Andersen, N.K. Tonks, N.P.H. Møller, Structural and evolutionary relationships among protein tyrosine phosphatase domains, Molecular and cellular biology, 21 (2001) 7117–7136.
24. T.R. Burke, K. Lee, Phosphotyrosyl mimetics in the development of signal transduction inhibitors, Accounts of chemical research, 36 (2003) 426–433.
25. P.J. Ala, L. Gonneville, M. Hillman, M. Becker-Pasha, E.W. Yue, B. Douty, B. Wayland, P. Polam, M.L. Crawley, E. McLaughlin, Structural insights into the design of nonpeptidic isothiazolidinone-containing inhibitors of protein-tyrosine phosphatase 1B, Journal of Biological Chemistry, 281 (2006) 38013–38021.
26. P.J. Ala, L. Gonneville, M.C. Hillman, M. Becker-Pasha, M. Wei, B.G. Reid, R. Klabe, E.W. Yue, B. Wayland, B. Douty, Structural basis for inhibition of protein-tyrosine phosphatase 1B by isothiazolidinone heterocyclic phosphonate mimetics, Journal of Biological Chemistry, 281 (2006) 32784–32795.
27. M. Sarmiento, L. Wu, Y.-F. Keng, L. Song, Z. Luo, Z. Huang, G.-Z. Wu, A.K. Yuan, Z.-Y. Zhang, Structure-based discovery of small molecule inhibitors targeted to protein tyrosine phosphatase 1B, Journal of medicinal chemistry, 43 (2000) 146–155.
28. Q. Wang, Z. Huang, C. Ramachandran, A.N. Dinaut, S.D. Taylor, Naphthalenebis [α, α-difluoromethylenephosphonates] as potent inhibitors of protein tyrosine phosphatases, Bioorganic & medicinal chemistry letters, 8 (1998) 345–350.
29. M. Taing, Y.-F. Keng, K. Shen, L. Wu, D.S. Lawrence, Z.-Y. Zhang, Potent and highly selective inhibitors of the protein tyrosine phosphatase 1B, Biochemistry, 38 (1999) 3793–3803.
30. E.J. Moran, S. Sarshar, J.F. Cargill, M.M. Shahbaz, A. Lio, A.M. Mjalli, R.W. Armstrong, Radio frequency tag encoded combinatorial library method for the discovery of tripeptide-substituted cinnamic acid inhibitors of the protein tyrosine phosphatase PTP1B, Journal of the American Chemical Society, 117 (1995) 10787–10788.
31. L. Cao, L. Zhang, P. Ruiz-Lozano, Q. Yang, K.R. Chien, R.M. Graham, M. Zhou, A novel putative protein-tyrosine phosphatase contains a BRO1-like domain and suppresses Ha-ras-mediated transformation, Journal of Biological Chemistry, 273 (1998) 21077–21083.
32. B. Ye, T.R. Burke Jr, Synthesis of a difluorophosphonomethyl-containing phosphatase inhibitor designed from the X-ray structure of a PTP1B-bound ligand, Tetrahedron, 52 (1996) 9963–9970.

33. T.R. Burke, B. Ye, X. Yan, S. Wang, Z. Jia, L. Chen, Z.-Y. Zhang, D. Barford, Small molecule interactions with protein – tyrosine phosphatase PTP1B and their use in inhibitor design, Biochemistry, 35 (1996) 15989–15996.
34. M. Dixit, U. Saeed, A. Kumar, M.I. Siddiqi, A.K. Tamrakar, A.K. Srivastava, A. Goel, Synthesis, molecular docking and PTP1B inhibitory activity of functionalized 4, 5-dihydronaphthofurans and dibenzofurans, (2008).
35. S. Liu, L.-F. Zeng, L. Wu, X. Yu, T. Xue, A.M. Gunawan, Y.-Q. Long, Z.-Y. Zhang, Targeting inactive enzyme conformation: aryl diketoacid derivatives as a new class of PTP1B inhibitors, Journal of the American Chemical Society, 130 (2008) 17075–17084.
36. C. Wiesmann, K.J. Barr, J. Kung, J. Zhu, D.A. Erlanson, W. Shen, B.J. Fahr, M. Zhong, L. Taylor, M. Randal, Allosteric inhibition of protein tyrosine phosphatase 1B, Nature structural & molecular biology, 11 (2004) 730–737.
37. M.S. Malamas, J. Sredy, I. Gunawan, B. Mihan, D.R. Sawicki, L. Seestaller, D. Sullivan, B.R. Flam, New azolidinediones as inhibitors of protein tyrosine phosphatase 1B with antihyperglycemic properties, Journal of medicinal chemistry, 43 (2000) 995–1010.
38. J. Wrobel, J. Sredy, C. Moxham, A. Dietrich, Z. Li, D.R. Sawicki, L. Seestaller, L. Wu, A. Katz, D. Sullivan, PTP1B inhibition and antihyperglycemic activity in the ob/ob mouse model of novel 11-arylbenzo [b] naphtho [2, 3-d] furans and 11-arylbenzo [b] naphtho [2, 3-d] thiophenes, Journal of medicinal chemistry, 42 (1999) 3199–3202.
39. M.K. Mahapatra, R. Kumar, M. Kumar, Synthesis, biological evaluation and in silico studies of 5-(3-methoxybenzylidene)thiazolidine-2,4-dione analogues as PTP1B inhibitors, Bioorg Chem, 71 (2017) 1–9.
40. M.K. Mahapatra, K. Bera, D.V. Singh, R. Kumar, M. Kumar, In silico modelling and molecular dynamics simulation studies of thiazolidine based PTP1B inhibitors, J Biomol Struct Dyn, 36 (2018) 1195–1211.
41. M.K. Mahapatra, R. Kumar, M. Kumar, N-alkylated thiazolidine-2,4-dione analogs as PTP1B inhibitors: synthesis, biological activity, and docking studies, Med Chem Res, 26 (2017) 1176–1183.
42. M.K. Gilson, T. Liu, M. Baitaluk, G. Nicola, L. Hwang, J. Chong, BindingDB in 2015: a public database for medicinal chemistry, computational chemistry and systems pharmacology, Nucleic acids research, 44 (2016) D1045-D1053.
43. W.L. DeLano, Pymol: An open-source molecular graphics tool, CCP4 Newsl. Protein Crystallogr, 40 (2002) 82–92.
44. J. Sunseri, D.R. Koes, Pharmit: interactive exploration of chemical space, Nucleic acids research, 44 (2016) W442-W448.
45. G. Landrum, Rdkit: Open-source cheminformatics software, 2016, URL http://www.rdkit.org/, https://github.com/rdkit/rdkit, 149 (2016) 150.
46. M.R. Berthold, N. Cebron, F. Dill, T.R. Gabriel, T. Kötter, T. Meinl, P. Ohl, K. Thiel, B. Wiswedel, KNIME-the Konstanz information miner: version 2.0 and beyond, AcM SIGKDD explorations Newsletter, 11 (2009) 26–31.
47. N.M. O'Boyle, M. Banck, C.A. James, C. Morley, T. Vandermeersch, G.R. Hutchison, Open Babel: An open chemical toolbox, Journal of Cheminformatics, 3 (2011) 33.
48. G.M. Morris, R. Huey, W. Lindstrom, M.F. Sanner, R.K. Belew, D.S. Goodsell, A.J. Olson, AutoDock4 and AutoDockTools4: Automated docking with selective receptor flexibility, Journal of computational chemistry, 30 (2009) 2785–2791.
49. J. Dowarah, V.P. Singh, Anti-diabetic drugs recent approaches and advancements, Bioorganic & Medicinal Chemistry, 28 (2020) 115263.
50. O. Trott, A.J. Olson, AutoDock Vina: improving the speed and accuracy of docking with a new scoring function, efficient optimization, and multithreading, Journal of computational chemistry, 31 (2010) 455–461.
51. T. Esaki, R. Ohashi, R. Watanabe, Y. Natsume-Kitatani, H. Kawashima, C. Nagao, H. Komura, K. Mizuguchi, Constructing an In Silico Three-Class Predictor of Human Intestinal Absorption With Caco-2 Permeability and Dried-DMSO Solubility, Journal of Pharmaceutical Sciences, 108 (2019) 3630–3639.

52. R. Watanabe, T. Esaki, R. Ohashi, M. Kuroda, H. Kawashima, H. Komura, Y. Natsume-Kitatani, K. Mizuguchi, Development of an In Silico Prediction Model for P-glycoprotein Efflux Potential in Brain Capillary Endothelial Cells toward the Prediction of Brain Penetration, Journal of Medicinal Chemistry, 64 (2021) 2725–2738.
53. R. Watanabe, T. Esaki, H. Kawashima, Y. Natsume-Kitatani, C. Nagao, R. Ohashi, K. Mizuguchi, Predicting Fraction Unbound in Human Plasma from Chemical Structure: Improved Accuracy in the Low Value Ranges, Molecular Pharmaceutics, 15 (2018) 5302–5311.
54. T. Esaki, R. Watanabe, H. Kawashima, R. Ohashi, Y. Natsume-Kitatani, C. Nagao, K. Mizuguchi, Data Curation can Improve the Prediction Accuracy of Metabolic Intrinsic Clearance, Molecular Informatics, 38 (2019) 1800086.
55. M.J. Abraham, T. Murtola, R. Schulz, S. Páll, J.C. Smith, B. Hess, E. Lindahl, GROMACS: High performance molecular simulations through multi-level parallelism from laptops to supercomputers, SoftwareX, 1 (2015) 19–25.
56. H. Fu, H. Zhang, H. Chen, X. Shao, C. Chipot, W. Cai, Zooming across the free-energy landscape: shaving barriers, and flooding valleys, The journal of physical chemistry letters, 9 (2018) 4738–4745.
57. D. Van Der Spoel, E. Lindahl, B. Hess, G. Groenhof, A.E. Mark, H.J.C. Berendsen, GROMACS: Fast, flexible, and free, Journal of Computational Chemistry, 26 (2005) 1701–1718.
58. H.M. Berman, J. Westbrook, Z. Feng, G. Gilliland, T.N. Bhat, H. Weissig, I.N. Shindyalov, P.E. Bourne, The protein data bank, Nucleic acids research, 28 (2000) 235–242.
59. P.J. Ala, L. Gonneville, M. Hillman, M. Becker-Pasha, E.W. Yue, B. Douty, B. Wayland, P. Polam, M.L. Crawley, E. McLaughlin, R.B. Sparks, B. Glass, A. Takvorian, A.P. Combs, T.C. Burn, G.F. Hollis, R. Wynn, Structural Insights into the Design of Nonpeptidic Isothiazolidinone-containing Inhibitors of Protein-tyrosine Phosphatase 1B*, Journal of Biological Chemistry, 281 (2006) 38013–38021.
60. D.P. Wilson, Z.-K. Wan, W.-X. Xu, S.J. Kirincich, B.C. Follows, D. Joseph-McCarthy, K. Foreman, A. Moretto, J. Wu, M. Zhu, E. Binnun, Y.-L. Zhang, M. Tam, D.V. Erbe, J. Tobin, X. Xu, L. Leung, A. Shilling, S.Y. Tam, T.S. Mansour, J. Lee, Structure-Based Optimization of Protein Tyrosine Phosphatase 1B Inhibitors: From the Active Site to the Second Phosphotyrosine Binding Site, Journal of Medicinal Chemistry, 50 (2007) 4681–4698.
61. B.G. Szczepankiewicz, G. Liu, P.J. Hajduk, C. Abad-Zapatero, Z. Pei, Z. Xin, T.H. Lubben, J.M. Trevillyan, M.A. Stashko, S.J. Ballaron, H. Liang, F. Huang, C.W. Hutchins, S.W. Fesik, M.R. Jirousek, Discovery of a Potent, Selective Protein Tyrosine Phosphatase 1B Inhibitor Using a Linked-Fragment Strategy, Journal of the American Chemical Society, 125 (2003) 4087–4096.
62. Z. Xin, T.K. Oost, C. Abad-Zapatero, P.J. Hajduk, Z. Pei, B.G. Szczepankiewicz, C.W. Hutchins, S.J. Ballaron, M.A. Stashko, T. Lubben, J.M. Trevillyan, M.R. Jirousek, G. Liu, Potent, selective inhibitors of protein tyrosine phosphatase 1B, Bioorg Med Chem Lett, 13 (2003) 1887–1890.
63. D.P. Wilson, Z.K. Wan, W.X. Xu, S.J. Kirincich, B.C. Follows, D. Joseph-McCarthy, K. Foreman, A. Moretto, J. Wu, M. Zhu, E. Binnun, Y.L. Zhang, M. Tam, D.V. Erbe, J. Tobin, X. Xu, L. Leung, A. Shilling, S.Y. Tam, T.S. Mansour, J. Lee, Structure-based optimization of protein tyrosine phosphatase 1B inhibitors: from the active site to the second phosphotyrosine binding site, J Med Chem, 50 (2007) 4681–4698.
64. D. Schneidman-Duhovny, O. Dror, Y. Inbar, R. Nussinov, H.J. Wolfson, PharmaGist: a webserver for ligand-based pharmacophore detection, Nucleic Acids Research, 36 (2008) W223-W228.
65. Akhilesh, A.T.K. Baidya, A. Uniyal, B. Das, R. Kumar, V. Tiwari, Structure-based virtual screening and molecular dynamics simulation for the identification of sphingosine kinase-2 inhibitors as potential analgesics, Journal of Biomolecular Structure and Dynamics, (2021) 1–19.
66. A.T. Baidya, A. Kumar, R. Kumar, T. Darreh-Shori, Allosteric Binding Sites of Aβ Peptides on the Acetylcholine Synthesizing Enzyme ChAT as Deduced by In Silico Molecular Modeling, International Journal of Molecular Sciences, 23 (2022) 6073.

67. J. Lee, X. Cheng, J.M. Swails, M.S. Yeom, P.K. Eastman, J.A. Lemkul, S. Wei, J. Buckner, J.C. Jeong, Y. Qi, CHARMM-GUI input generator for NAMD, GROMACS, AMBER, OpenMM, and CHARMM/OpenMM simulations using the CHARMM36 additive force field, Journal of chemical theory and computation, 12 (2016) 405–413.
68. D.J. Evans, B.L. Holian, The nose–hoover thermostat, The Journal of chemical physics, 83 (1985) 4069–4074.
69. M. Parrinello, A. Rahman, Polymorphic transitions in single crystals: A new molecular dynamics method, Journal of Applied physics, 52 (1981) 7182–7190.
70. M.S. Valdés-Tresanco, M.E. Valdés-Tresanco, P.A. Valiente, E. Moreno, gmx_MMPBSA: A New Tool to Perform End-State Free Energy Calculations with GROMACS, Journal of Chemical Theory and Computation, 17 (2021) 6281–6291.

Figures

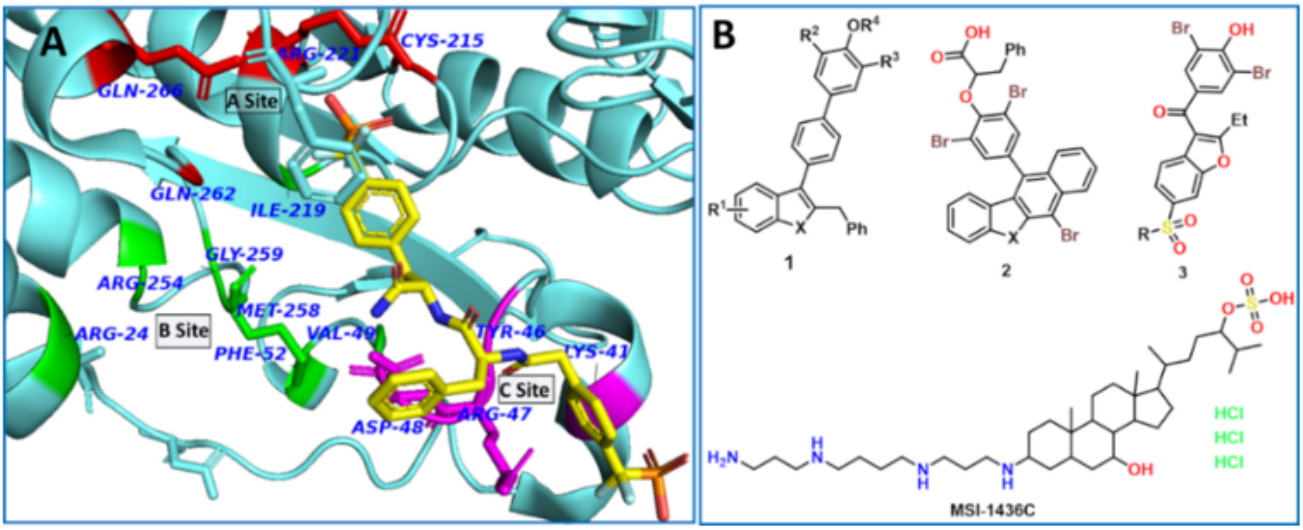

Figure 1

A) Sub pockets of active site of PTP1B enzyme with highlighted amino acids in red (A site), green (B site) and magenta (C site); B) examples of some reported PTP1B Inhibitors.

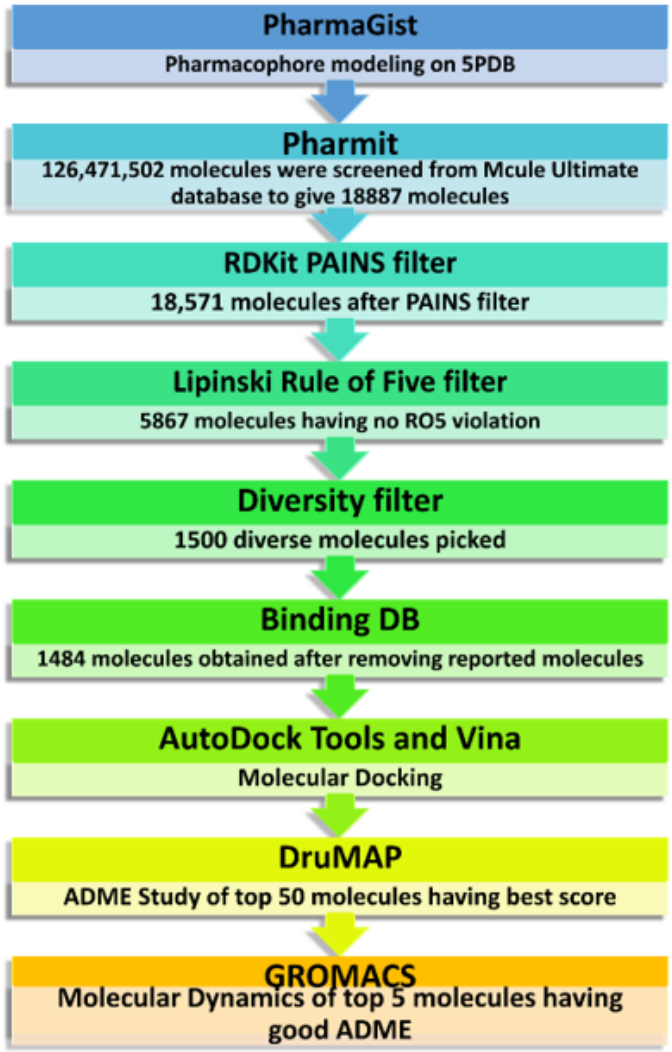

Figure 2

Workflow used for pharmacophore followed by structure based virtual screening

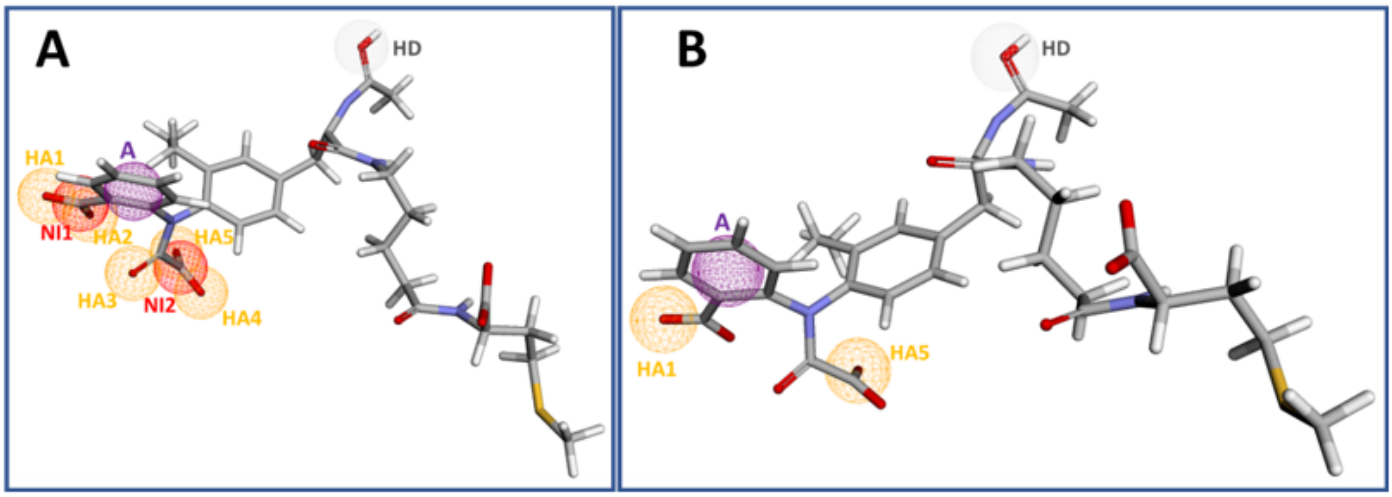

Figure 3

Pharmacophore model for PTP1B inhibitor A) Pharmacophore model generated by overlapping five different inhibitors of PTP1B with five hydrogen acceptors (HA, orange sphere), two negative ions (N, red sphere), one aromatic (A, purple sphere) and 1 hydrogen donor (HD, light grey sphere). B) Pharmacophoric model used for pharmacophore based virtual screening containing 2 hydrogen acceptors, 1 aromatic and 1 hydrogen donor.

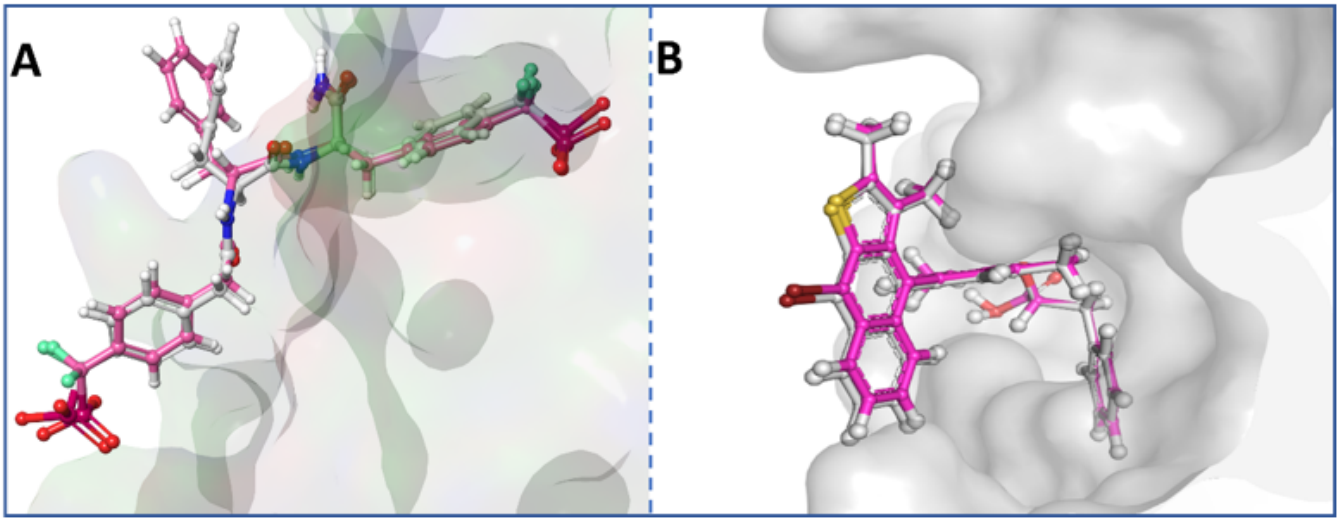

Figure 4

Superimposition of co-crystallized ligand (A) and Ertiprotafib (B) on redocking inside the binding pocket of PTP1B enzyme (PDB Id 2CNE).

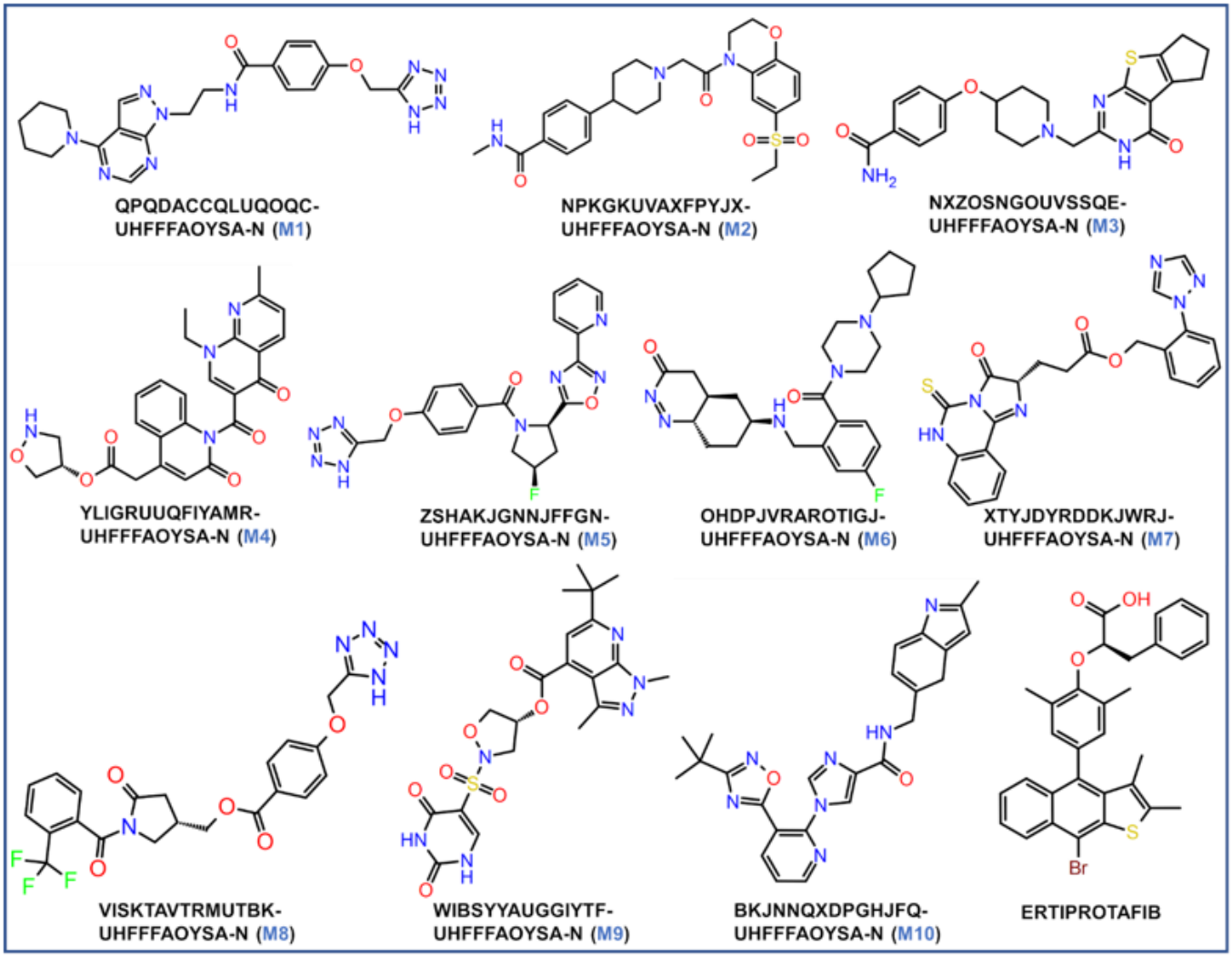

Figure 5

2D structures of top ten hits obtained after virtual screening and ADME studies along with the standard PTP1B inhibitor Ertiprotafib

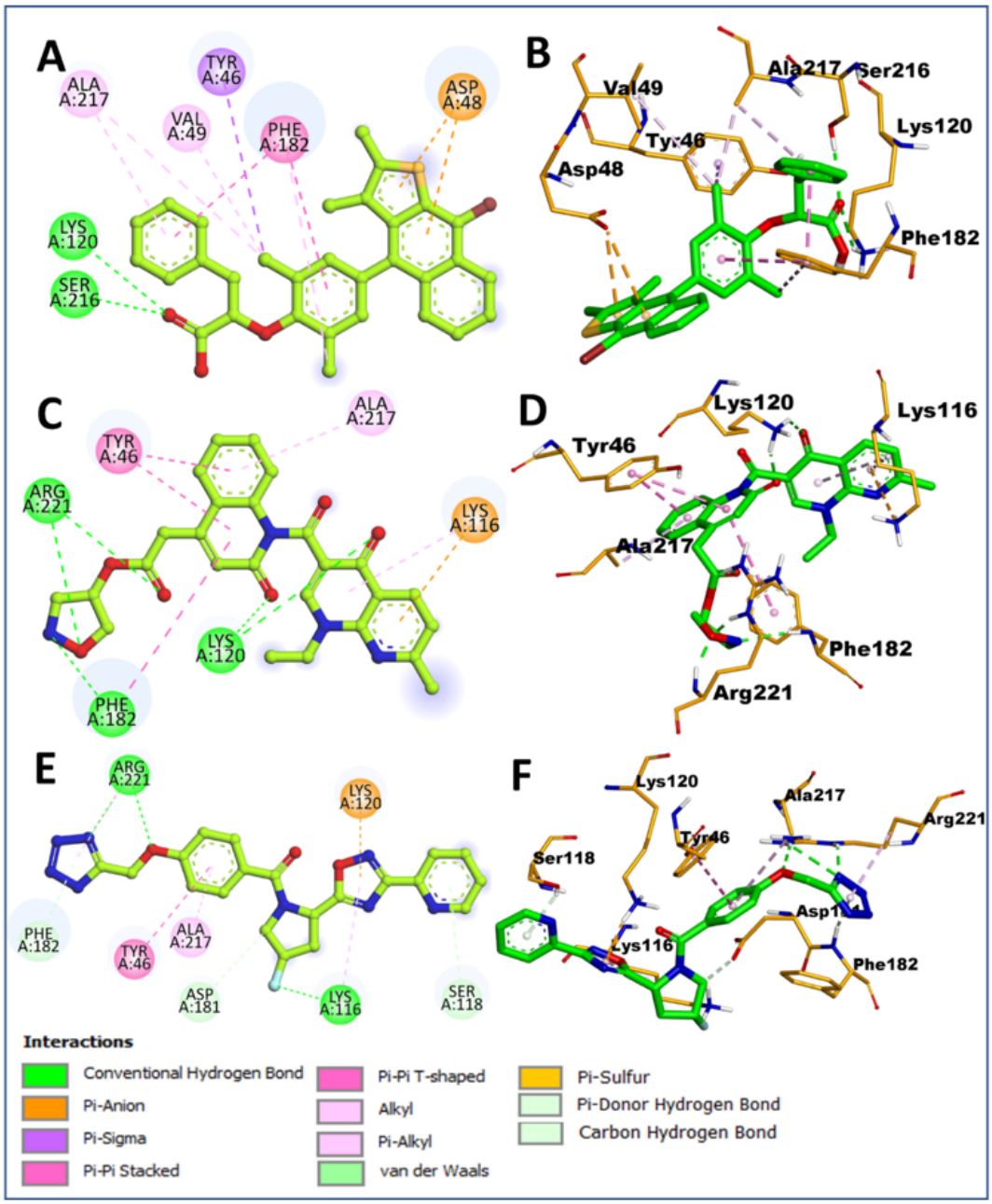

Figure 6

Interaction representation of Ertiprotafib and top hits. Left column and right columns represents 2D and 3D interaction diagrams. A and B) Ertiprotafib; C and D) Compound M4; E and F) Compound M5

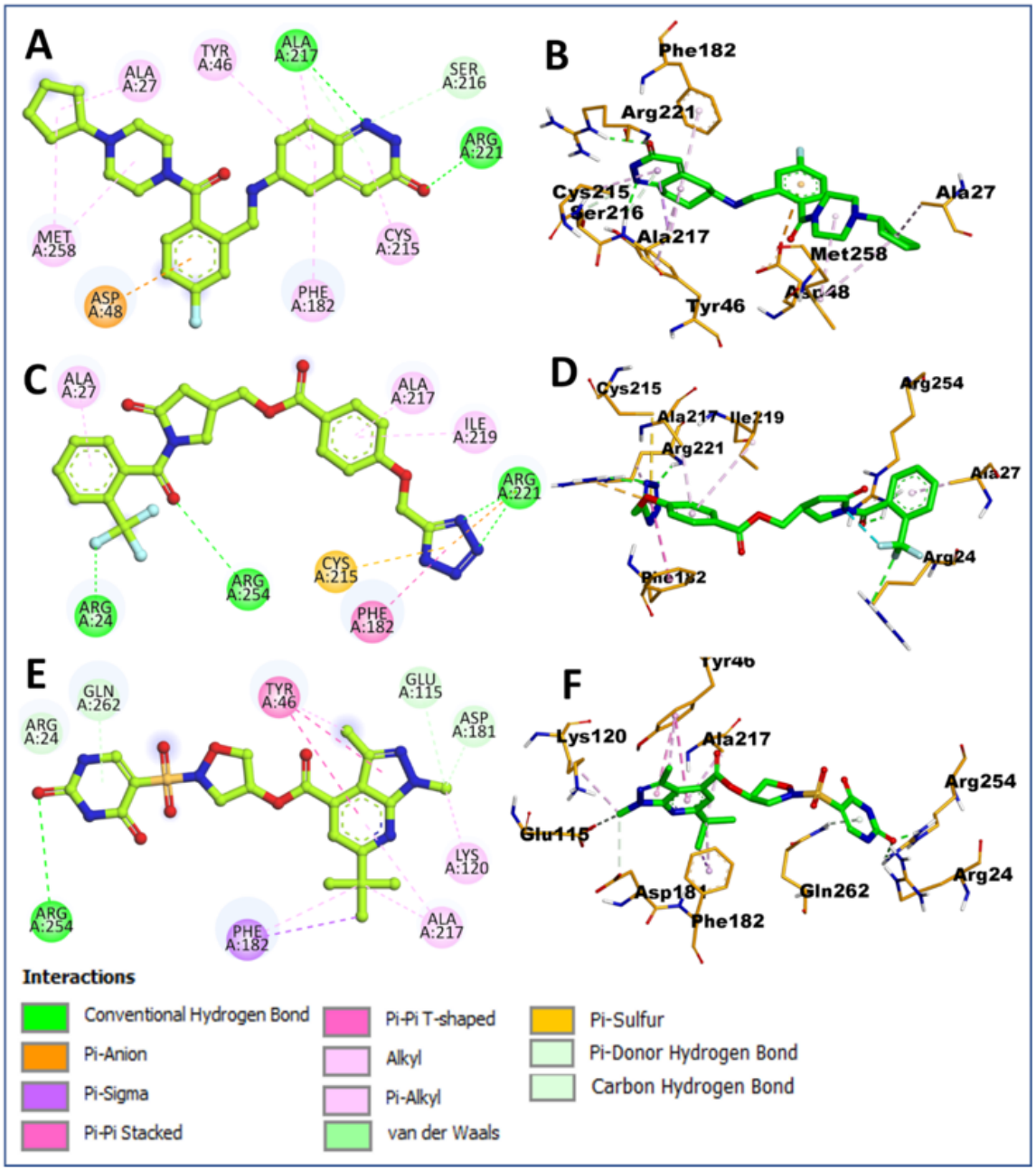

Figure 7

Interaction representation of best pose of top hits with PTP1B protein after docking with vina software. Left column and right columns represents 2D and 3D interaction diagrams. A and B) Compound M6; C and D) Compound M8; E and F) Compound M9

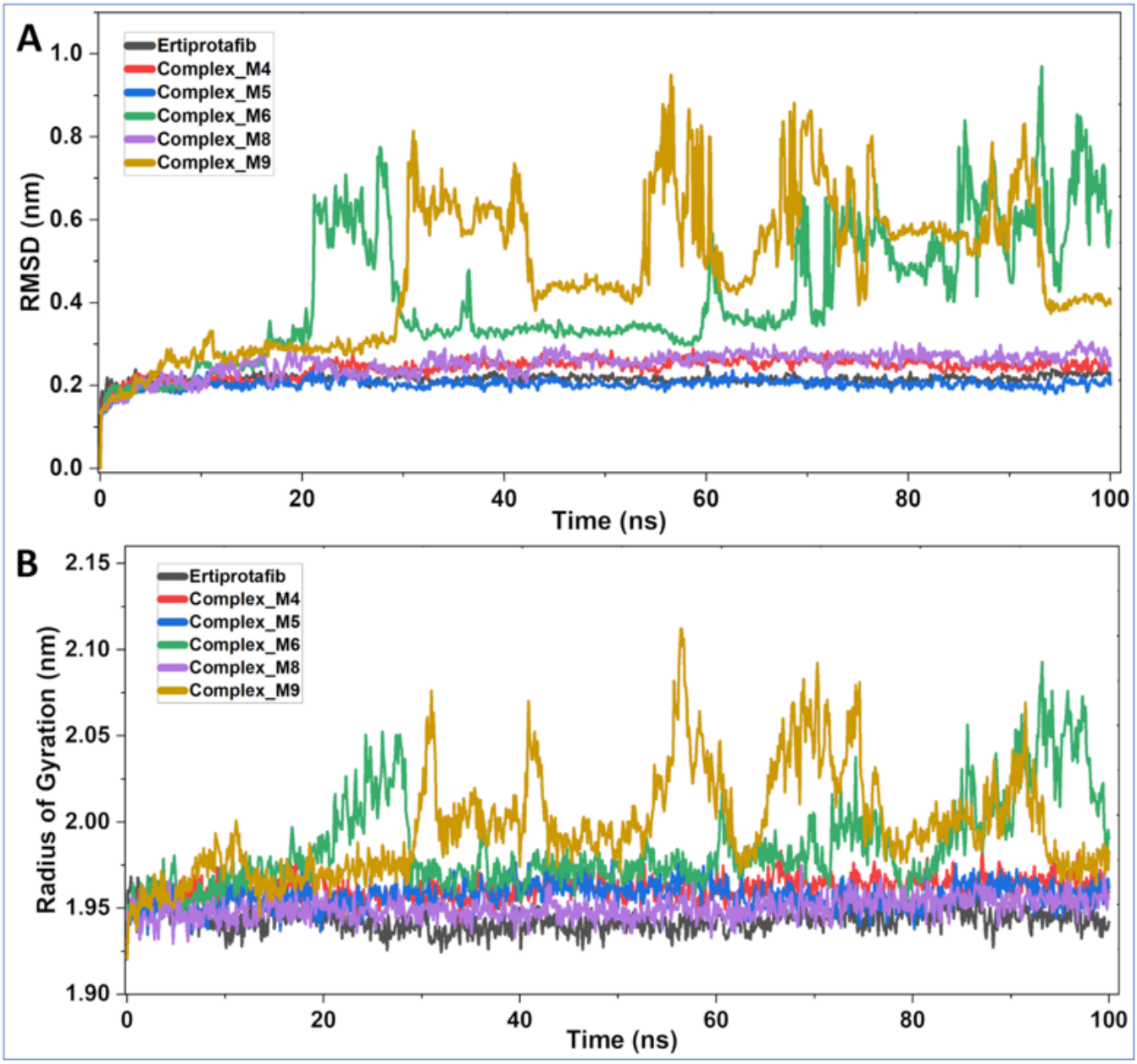

Figure 8

MD trajectory analysis displaying A) RMSD and B) rGy calculated after 100ns of MD simulation for all six compounds with PTP1B protein

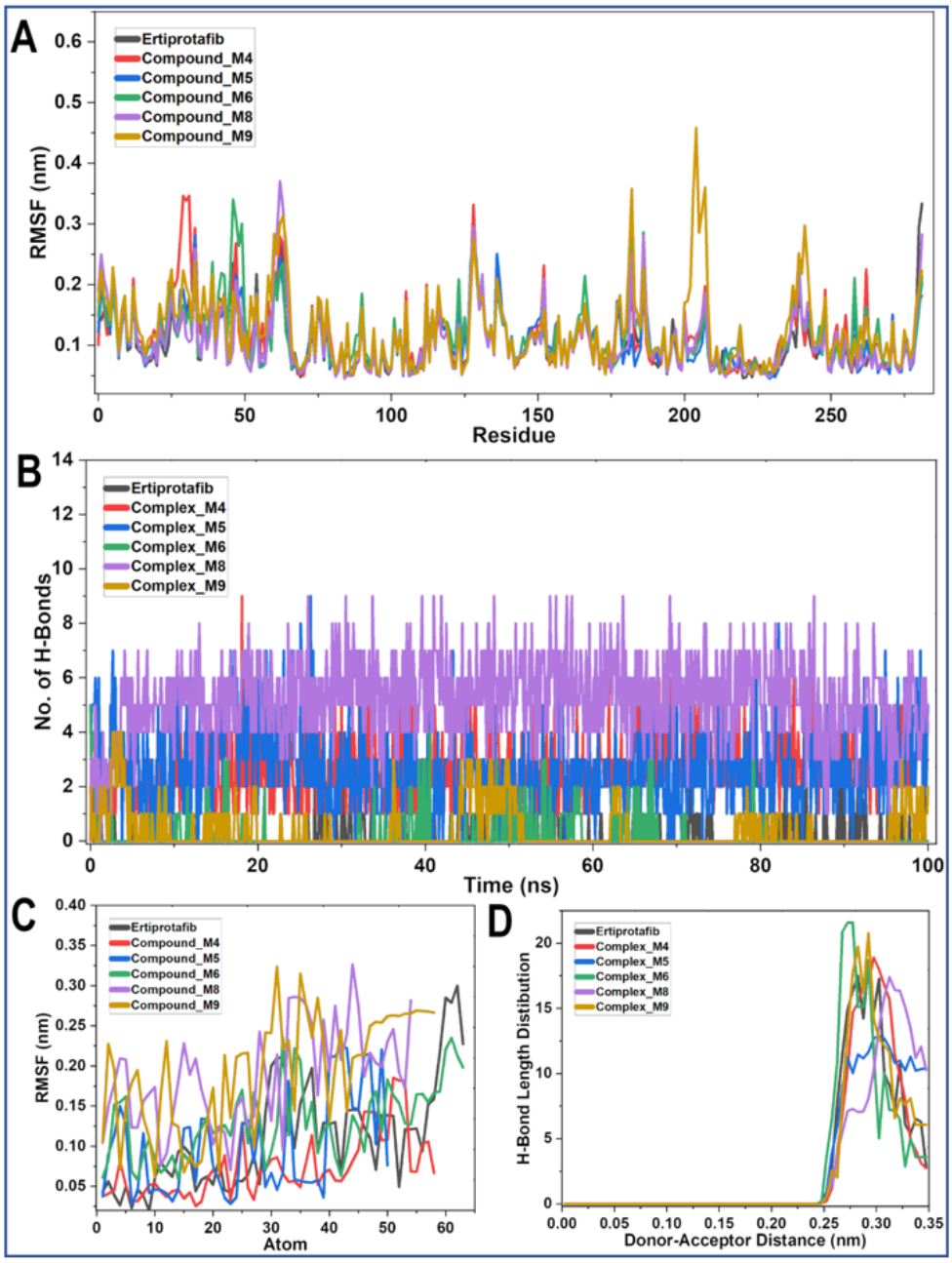

Figure 9

MD trajectory analysis displaying A) RMSF for PTP1B protein, B) Number of hydrogen bond, C) RMSF for ligands, and D) Hydrogen bond length distribution throughout the 100ns of MD simulation.

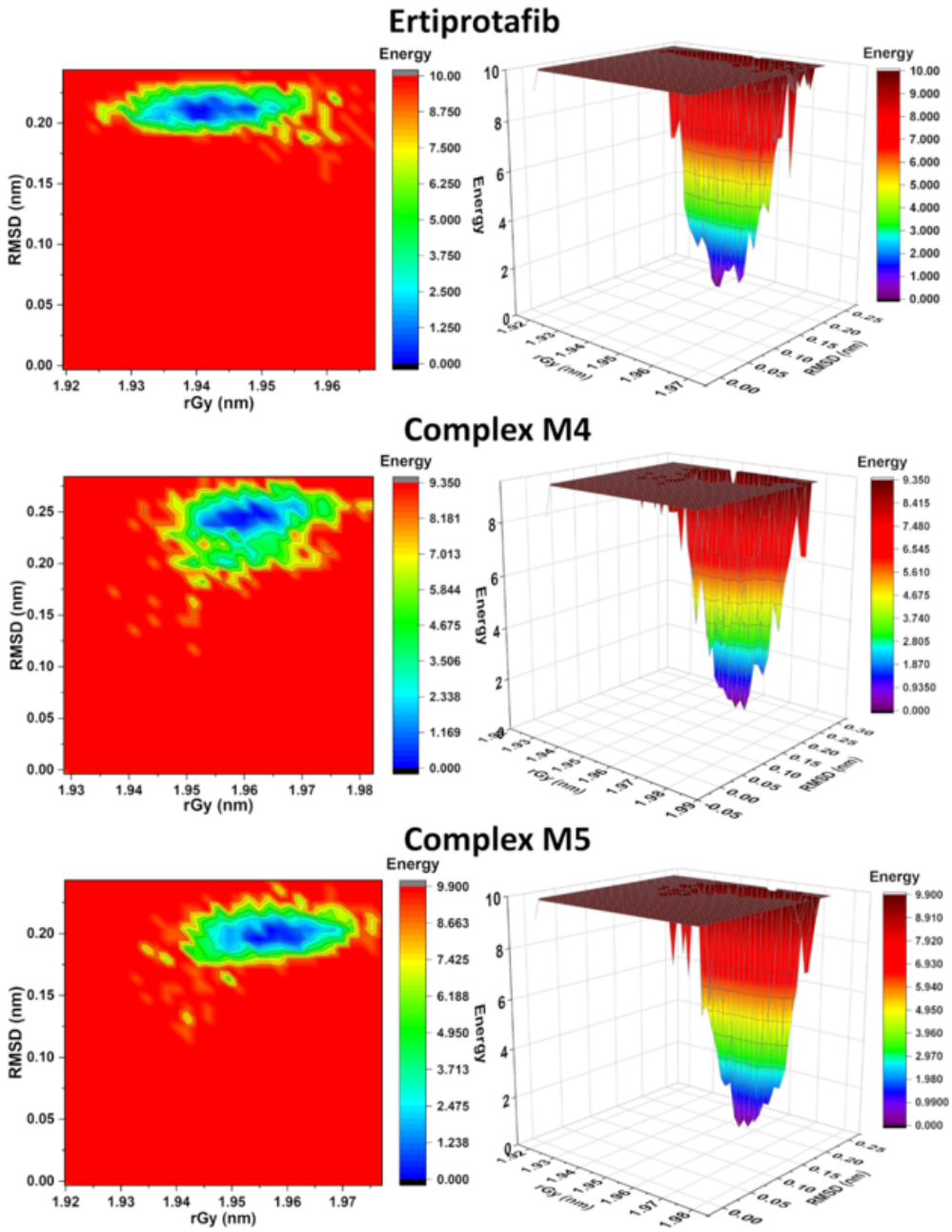

Figure 10

The 2D and 3D free energy landscape diagram of PTP1B-Ligand Complex as a function of RMSD and rGy as the two variables. The topography represents low free energy regions in blue and metastable states in dark red. Here, all three compounds showed one stable folding stable corresponding to blue region.

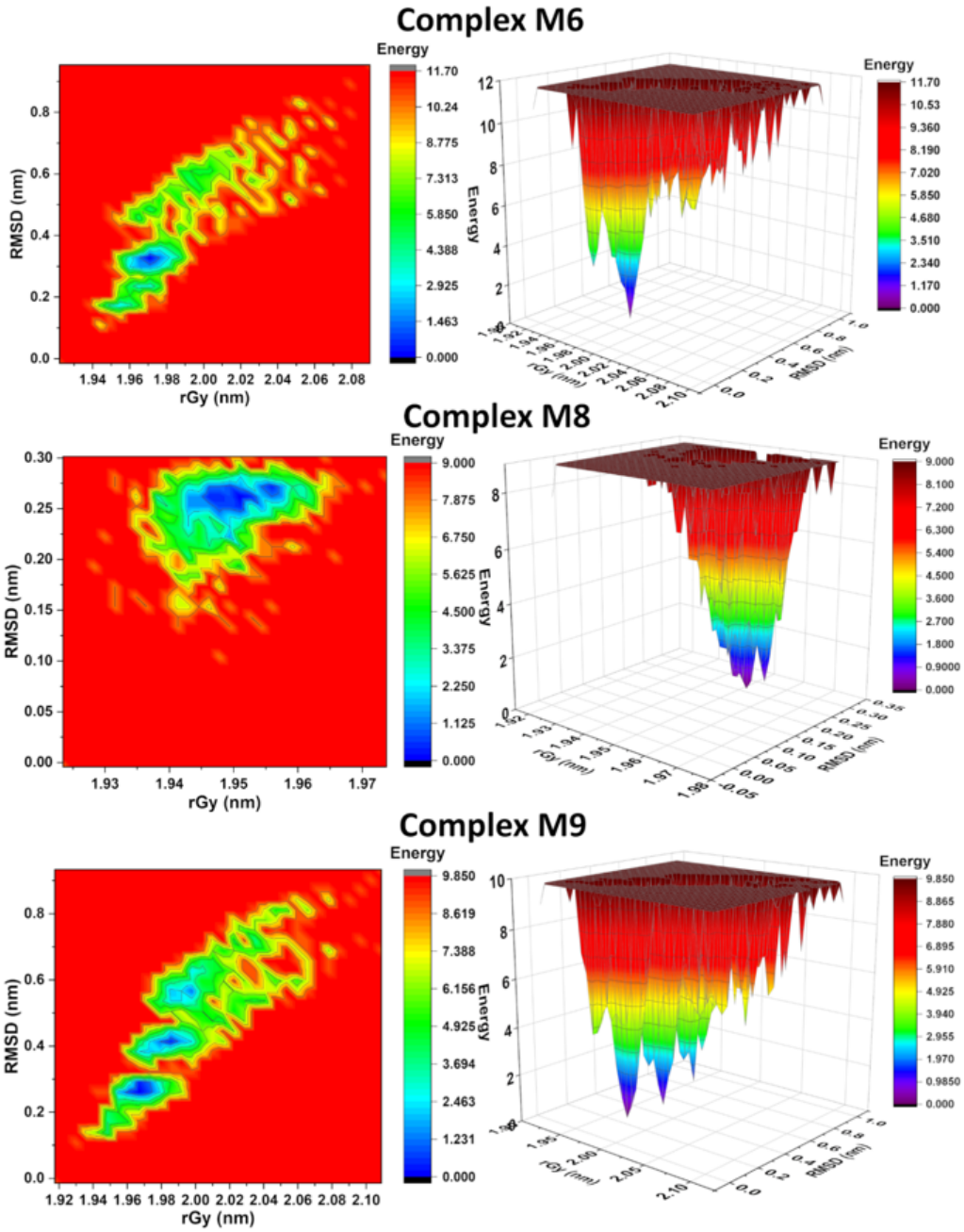

Figure 11

The 2D and 3D free energy landscape diagram of PTP1B-Ligand Complex as a function of RMSD and rGy as the two variables. The topography represents low free energy regions in blue and metastable states in dark red. Here, Compound M6 showed one stable folding state while other two (M8 and M9) has more than one stable folding state.

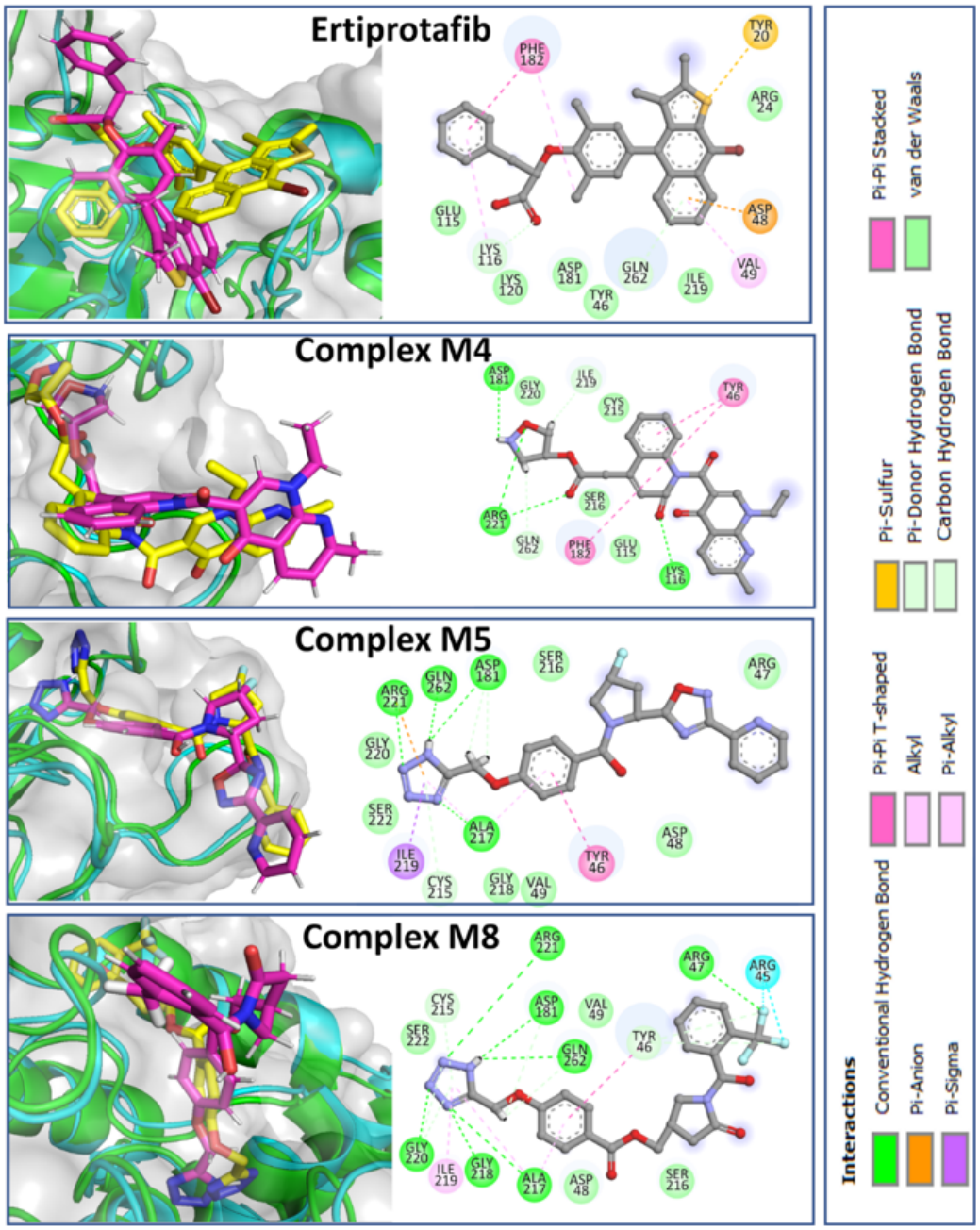

Figure 12

Interactions and Binding Pose of Compounds after MD studies. In binding pose, yellow and magenta colored structure represent the ligand pose before (docked) and after MD respectively.

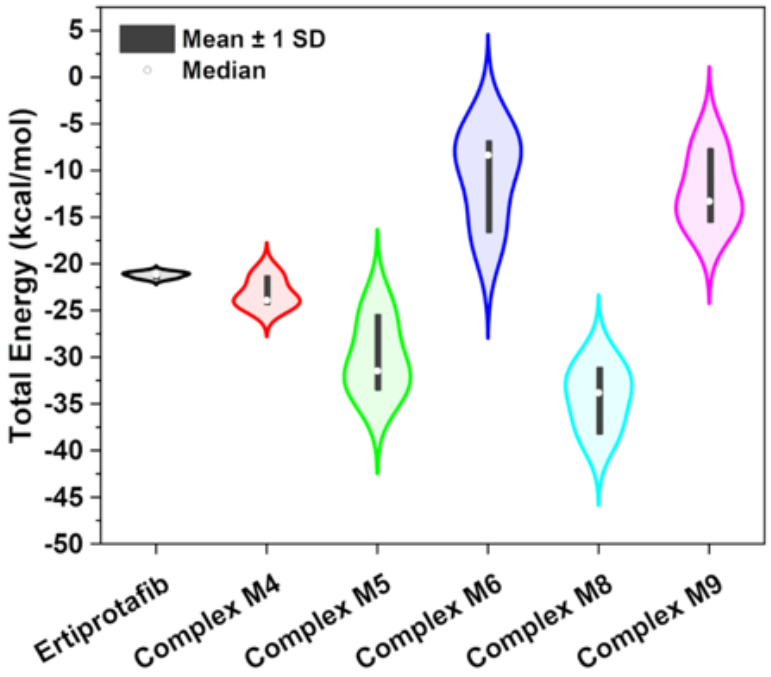

Figure 13

Violin plot for the *In silico* calculated Binding Free Energy, ΔG (kcal/mol) by MM-PBSA.

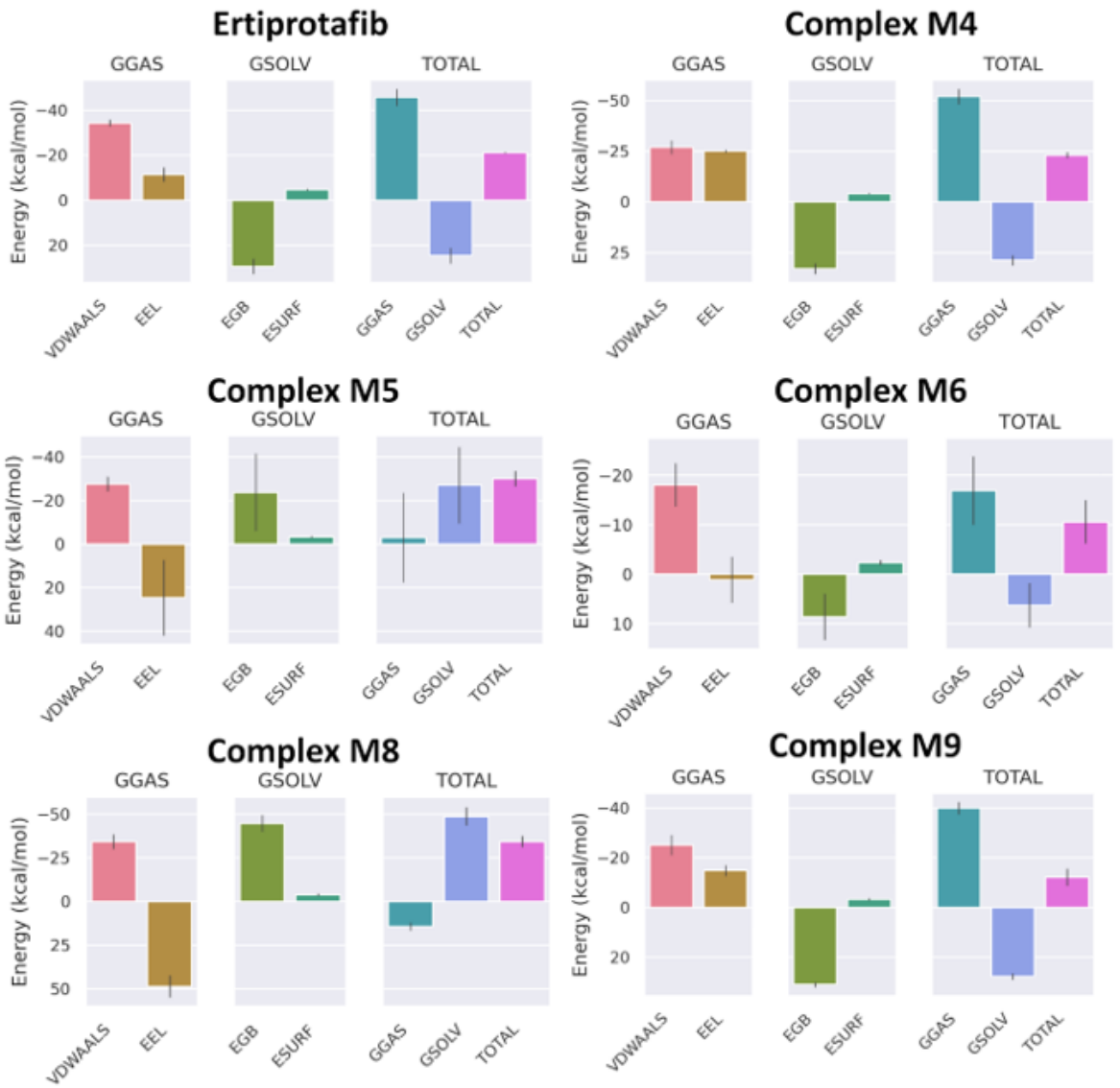

Figure 14

Contribution of Individual component in the Total Binding Free Energy, ΔG (kcal/mol) energy for each complex calculated by MM-PBSA.